Anal. Chem. **2009,** *81,* 5740–5748

Nanoporous Membranes with Mixed Nanoclusters for Raman-Based Label-Free Monitoring of Peroxide Compounds

Sehoon Chang, Hyunhyub Ko,† Srikanth Singamaneni, Ray Gunawidjaja, and Vladimir V. Tsukruk*

School of Materials Science and Engineering and School of Polymer, Textile, and Fiber Engineering, Georgia Institute of Technology, Atlanta, Georgia 30332

Monitoring trace amounts of peroxide-based molecules is challenging because of the lack of common optical signatures (fluorescence or absorption in UV−vis range) or chemical functionality easily detectable with common routines. To overcome this issue, we suggest a photochemical decomposition approach followed by the analysis of chemical fragments by a fast, sensitive, and reliable Raman spectroscopic method. To facilitate this approach, we employed a novel design of surface-enhanced Raman scattering (SERS)-active nanoporous substrate based on porous alumina membranes decorated with mixed nanoclusters composed of gold nanorods and nanoparticles. The detectable amount of HMTD below 2 pg demonstrated here is about 3 orders of magnitude lower than the current limit of detection. We suggest that laser-induced photocatalytic decomposition onto nanoparticle clusters is critical for achieving label-free detection of unstable and nonresonant organic molecules.

INTRODUCTION

Surface-enhanced Raman scattering (SERS) has emerged as a powerful analytical technique for the detection of trace levels (down to a single molecule under ideal conditions) of chemical and biological analytes because of high sensitivity, selectivity, rapid response, and portability. SERS results in the dramatic enhancement of the intensity of the Raman spectra of the analyte adsorbed on metal nanostructures. While the SERS enhancement is believed to be caused by two distinct factors, namely, electromagnetic and chemical enhancements, the former is considered to contribute several orders of magnitude (6−8) higher enhancement than that of the latter.[1−3] The large enhancement of the near field in the interstices of closely separated (a few nanometers) metal nanostructures, often termed as *hot spots*, is responsible for the large enhancement of scattering cross-sections. SERS-based chemical and biological sensors have been applied for the trace level detection of various hazardous chemicals such as pesticides,[4] toxins,[5] nuclear waste,[6] biomolecules,[7] and explosives.[8] The sensing results demonstrated to date are comparable to those reported for another robust practical detection routine based upon microcantilever arrays.[9,10]

To date, a variety of nanostructured SERS-active substrates have been suggested to enhance Raman-based detection such as roughened metal surfaces, nanoislands, nanoparticles, hole arrays, and nanoshells as discussed in a number of recent reviews and original publications.[11−17] However, the ability of SERS chemical sensors to detect small, nonresonant organic molecules such as those belonging to important hazardous chemicals and explosives is still very limited. Rapid detection of peroxide-based liquid explosives such as hexamethylenetriperoxidediamine (HMTD) is an urgent need because of recent security threats.

Because peroxide-based explosives have no color, flavor, or tactile characteristics, it is difficult to monitor their trace amounts by conventional analytical tools. It is even more challenging because of the lack of specific chemical functionalities such as amino groups or aromatic functional groups, absence of significant light absorption in UV−vis region, or a strong fluorescence signal.[18] Although infrared and mass spectroscopy techniques have been employed for the detection of these compounds, these methods are not feasible for in-field use because they are plagued

* Corresponding author. E-mail: vladimir@mse.gatech.edu.

† Current address: Department of Electrical Engineering and Computer Sciences, University of California at Berkeley, CA 94720.

(1) Kneipp, K. *Phys. Today* **2007**, *60*, 40–46.
(2) Nie, S.; Emory, S. R. *Science* **1997**, *275*, 1102–1106.
(3) Le Ru, E. C.; Blackie, E.; Meyer, M.; Etchegoin, P. G. *J. Phys. Chem. C* **2007**, *111*, 13794–13803.
(4) Alvarez-ros, M. C.; Sanchez-Sortes, S.; Francioso, O.; Garcia-Ramos, J. V. *Can. J. Anal. Sci. Spectrosc.* **2003**, *48*, 132–138.
(5) Spencer, K. M.; Sylvia, J. M.; Clauson, S. L.; Christensen, S. D. *Proc. SPIE Int. Soc. Opt. Eng.* **2004**, *5268*, 340–348.
(6) Bao, L.; Mahurin, S. M.; Haire, R. G.; Dai, S. *Anal. Chem.* **2003**, *75*, 6614–6620.
(7) Kumar, G. V. P.; Shruthi, S.; Vibha, B.; Ashok Reddy, B. A.; Kundu, T. K.; Narayana, C. *J. Phys. Chem. C* **2007**, *111*, 4388–4392.
(8) Bertone, J. F.; Cordeiro, K. L.; Sylvia, J. M.; Spencer, K. M. *Proc. SPIE Int. Soc. Opt. Eng.* **2004**, *5403*, 387–394.
(9) Singamaneni, S.; LeMieux, M. C.; Lang, H. P.; Gerber, Ch.; Lam, Y,; Zauscher, S.; Datskos, P. G.; Lavrik, N. V.; Jiang, H.; Naik, R. R.; Bunning, T. J.; Tsukruk, V. V. *Adv. Mater.* **2008**, *20*, 653–680.
(10) Singamaneni, S.; McConney, M. E.; LeMieux, M. C.; Jiang, H.; Enlow, J. O.; Bunning, T. J.; Naik, R. R.; Tsukruk, V. V. *Adv. Mater.* **2007**, *19*, 4248–4255.
(11) Moskovots, M. *Rev. Mod. Phys.* **1985**, *57*, 783–826.
(12) Ko, H.; Singamaneni, S.; Tsukruk, V. V. *Small* **2008**, *4*, 1576–1599.
(13) Stewart, M. E.; Anderton, C. R.; Thompson, L. B.; Maria, J.; Gray, S. K.; Rogers, J. A.; Nuzzo, R. G. *Chem. Rev.* **2008**, *108*, 494–521.
(14) Willets, K. A.; Van Duyne, R. P. *Annu. Rev. Phys. Chem.* **2007**, *58*, 267–297.
(15) Schatz, G. C.; Young, M. A.; Van Duyne, R. P. *Appl. Phys.* **2006**, *103*, 19–46.
(16) Banholzer, M. J.; Millstone, J. E.; Qin, L. D.; Mirkin, C. A. *Chem. Soc. Rev.* **2008**, *37*, 885–897.
(17) Jiang, C.; Lio, W. Y.; Tsukruk, V. V. *Phys. Rev. Lett.* **2005**, *95*, 115503–4.
(18) Cotte-Rodríguez, I.; Chen, H.; Cooks, R. G. *Chem. Commun.* **2006**, *9*, 953–955.

10.1021/ac900537d CCC: $40.75
Published on Web 06/11/2009

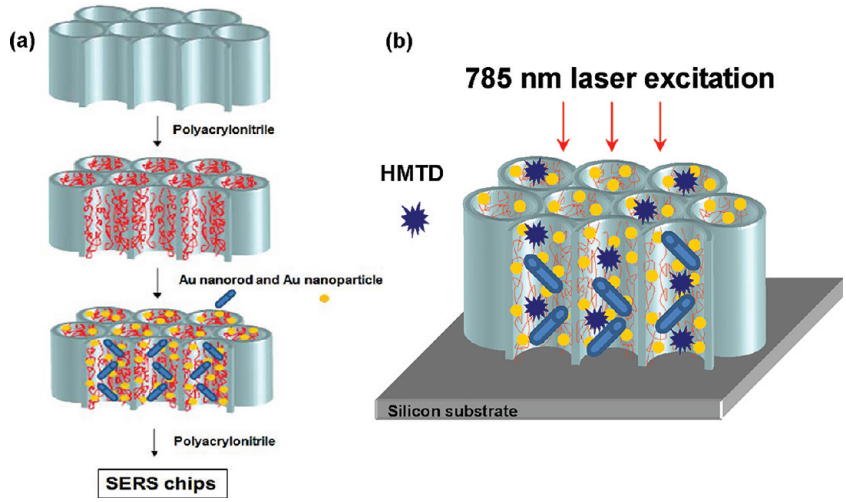

Figure 1. (a) Fabrication of 3D porous alumina membrane substrates and (b) chemical detection with Raman spectroscopy.

by low sensitivity and slow response. Alternatively, electrochemical, liquid chromatography with electrospray ionization mass spectroscopy and atmospheric pressure chemical ionization mass spectroscopy,[19−22] liquid chromatography with fluorescence, and desorption electrospray ionization techniques have been investigated for the detection of HMTD compounds.[18,19,23,24] The critical drawback of chromatographic separation as a sensing application is the long sample preparation time, which makes it unsuitable for quick screening and field testing. Although the decomposition of a chemical species under laser irradiation depending on laser energy, laser power, and exposure duration is a well-known approach, it is rarely utilized for trace detection with a "field-friendly" SERS technique.[25]

The occurrence of the plasmon resonance of Au and Ag in the visible region makes the nanostructures of these metals the most common choice for colorimetric-based chemical sensors.[12,26−29] Gold nanorods offer various advantages over nanoparticles which can be utilized for sensing.[30,31] For example, the longitudinal plasmon band of gold nanorods can be easily tuned by changing the aspect ratio to match the excitation laser for the maximum Raman enhancement.[32] In addition, gold nanorods can be instrumental for the realization of hot spots because the sharp edges of the individual nanorod can give rise to large electromagnetic enhancement. Moreover, mixed nanostructures such as gold nanorods combined with nanoparticles have been demonstrated to show even higher SERS enhancement compared to the nanoparticles alone.[33]

Here, we report on a novel nanoporous SERS-active substrate based on porous alumina membranes (PAMs)[34] decorated with mixed nanoclusters, which demonstrates trace level monitoring of peroxide-based liquid explosive, HMTD (Figure 1). The key design criterion of the SERS substrates suggested here is the utilization of selective polymer nanocoating combined with noble metal nanostructured aggregates within cylindrical nanopores for the capture and decomposition of analyte molecules.[34−36] The mechanism of photolysis of peroxide bonds to generate radicals has been reported but rarely utilized for real-time peroxide monitoring with practical, meaningful sensitivity.[37,38]

EXPERIMENTAL METHODS

Gold Nanoparticle and Gold Nanorod Synthesis. Gold nanoparticles of about 30 nm in diameter capped with cetyltrimethylammonium bromide (CTAB) were synthesized by a seed growth technique.[39] Gold nanorods have been synthesized using a seed-mediated growth technique introduced by Murphy et al. and El-Sayed et al.[32,40,41] Gold nanoparticle seed solution was prepared by addition of 0.6 mL of an ice-cold solution of 10 mM sodium borohydride into 10 mL of 2.5×10^{-4} M $HAuCl_4$ aqueous solution. It is worth noting that the gold chloride solution containing HCl did not produce the desired seeds. A 0.1 M cetyltrimethylammonium (CTAB) solution was added during

(19) Widmer, L.; Watson, S.; Scholatter, K.; Crowon, A. *Analyst* **2002**, *127*, 1627–1632.
(20) Zitrin, S.; Kraus S.; Glattstein, B. Proceedings of the International Symposium on the Analysis and Detection of Explosives, Quantico, VA, FBI: Washington, DC, 1983, pp 137−141.
(21) Evans, H. K.; Tulleners, F. A. J.; Sanchez, B. L.; Rasmussen, C. A. *J. Forensic Sci.* **1986**, *31*, 1119–1125.
(22) White, G. M. *J. Forensic Sci.* **1992**, *37*, 652–656.
(23) Bannister, W. W.; Chen, C.-C.; Curby, W. A.; Chen, E. B.; Damour, P. L.; Morales, A. US Patent 6406918 B1, 2002.
(24) Schulte-Ladbeck, R.; Kolla, P.; Karst, U. *Anal. Chem.* **2003**, *75*, 731–735.
(25) Reichardt, C.; Schroeder, J.; Schwarzer, D. P. *Phys. Chem. Chem. Phys.* **2008**, *10*, 5218–5220.
(26) Ren, B.; Liu, G. K.; Lian, X. B.; Yang, Z.-L.; Tian, Z.-Q. *Anal. Bioanal. Chem.* **2007**, *388*, 29–45.
(27) Cline, M. P.; Barber, P. W.; Chang, R. K. *J. Opt. Soc. Am. B: Opt. Phys.* **1986**, *3*, 15–21.
(28) Chen, X.; Narayanan, R.; El-Sayed, M. A. *Chem. Rev.* **2005**, *105*, 1025–1102.
(29) Jiang, C.; Markutsya, S.; Tsukruk, V. V. *Langmuir* **2004**, *20*, 882–890.
(30) Huang, X.; El-Sayed, I. H.; Qian, W.; El-Sayed, M. A. *Nano Lett.* **2007**, *7*, 1591–1597.
(31) Kozlovskaya, V.; Kharlampieva, E.; Khanal, B. P.; Manna, P.; Zubarev, E. R.; Tsukruk, V. V. *Chem. Mater.* **2008**, *20*, 7474–7485.
(32) Nikoobakht, B.; El-Sayed, M. A. *Chem. Mater.* **2003**, *15*, 1957–1962.
(33) Nikoobakht, B.; El-Sayed, M. A. *J. Phys. Chem. A* **2003**, *107*, 3372–3378.
(34) Ko, H.; Tsukruk, V. V. *Small* **2008**, *4*, 1980–1984.
(35) Saito, M.; Shibasaki, M.; Nakamura, S.; Miyagi, M. *Opt. Lett.* **1994**, *19*, 710–713.
(36) Lau, K. H. A.; Tan, L.-S.; Tamada, K.; Sander, M. S.; Knoll, W. *J. Phys. Chem. B* **2004**, *108*, 10812–10818.
(37) Frost, G. J.; Ellison, G. B.; Vaida, V. *J. Phys. Chem. A* **1999**, *103*, 10169–10178.
(38) Lunak, S.; Sedak, P. *J. Photochem. Photobiol. A: Chem.* **1992**, *68*, 1–8.
(39) Kwon, K.; Lee, K. Y.; Lee, Y. W.; Kim, M.; Heo, J.; Ahn, S. J.; Han, S. W. *J. Phys. Chem. C* **2007**, *111*, 1161–1165.
(40) Gole, A.; Murphy, C. J. *Langmuir* **2008**, *24*, 266–272.
(41) Lee, K. S.; El-Sayed, M. A. *J. Phys. Chem. B* **2005**, *109*, 20331–20338.

10 min of stirring. The color of the seed solution changed from yellow to brown. To make the growth solution, 95 mL of 0.1 M CTAB solution, 1 mL of 10 mM silver nitrate solution, and 5 mL of 10 mM $HAuCl_4$ solution were mixed, and 0.55 mL of 0.1 M ascorbic acid solution was added. Finally, 0.12 mL of seed solution was added to the growth solution. The final solution was left overnight, and the color turned orange-brown. The gold nanorod solution was centrifuged two times at 5000 rpm for 1 h each to remove excess CTAB.

3D SERS Substrate Design. Porous alumina membranes (PAMS) with a pore diameter of 250 nm and a 60 μm thickness were purchased from Whatman (Anodisc 47). Polyacrylonitrile (PAN) which was employed as a selective coating was dissolved in *N*,*N*-dimethylformamide (DMF) at 100 °C. A 0.2% PAN in DMF solution was spin-cast (4000 rpm, 30 s) on PAM and rinsed with DMF two times for gold nanorod attachment. The gold solution was filtered through a porous alumina membrane several times to achieve a uniform coating inside the PAMs.[34] After this step, 0.1% PAN in DMF was spin-cast (4000 rpm, 30 s) one more time to immobilize gold nanoparticles inside the pores.

Raman Measurements. Raman spectra of HMTD (Accustandard) were collected with a Holoprobe Raman microscope (Hololab series 5000 spectrometer, Kaiser Optical Systems) with backscattered configuration using 10× objective lens. A diode laser with 785 nm wavelength was used as an excitation laser source. A 10 μL amount of HMTD in acetonitrile with the desired concentration was dropped and evaporated on a 1 × 1 cm^2 area of the SERS substrate. For each sample, four points were collected with a 20 s acquisition time at different locations and averaged. The peak assignment of the Raman spectra obtained was performed by a computational library, Advanced Chemistry Development (ACD). The analyte molecules (input to ACD) for assigning the vibrational bands included HMTD, PAN, and CTAB molecules, and the possible decomposed compounds and peak positions were verified against standard Raman databases.[42,43]

A field-emission scanning electron microscopy (FESEM, LEO 1530) was used to investigate the assembly of gold nanoparticles and nanorods on PAMs. Transmission electron microscopy (TEM) (JEOL 100CX-2 electron microscope) was used at 100 kV to analyze the size and shape of the gold nanorods. We used optical microscopy (LEICA DM4000) to analyze HMTD aggregation on the polymer-selective coating. UV−vis measurement of gold nanorod solution and various PAMs was carried out by using a Creig spectrophotometer attached to LEICA Microsystem DM4000. The effective thickness of polymer coating was determined with a Woolam M2000U spectroscopic ellipsometer.

To analyze decomposed molecules of HMTD, XPS was performed on an M-PROBE Surface Science XPS spectrometer using charge neutralization. Spectra were collected from 0 to 1000 eV at 1 eV steps at a spot size of 800 um and averaged over 15 scans. FTIR spectra were collected using a Bruker FTIR spectrometer equipped with a narrow-band mercury cadmium telluride detector. The ATR surface was a rectangular trapezoidal Si crystal of dimension 50 mm × 20 mm × 2 mm (Harrick Scientific) whose beam entrance and exit surfaces were cut at 45°.

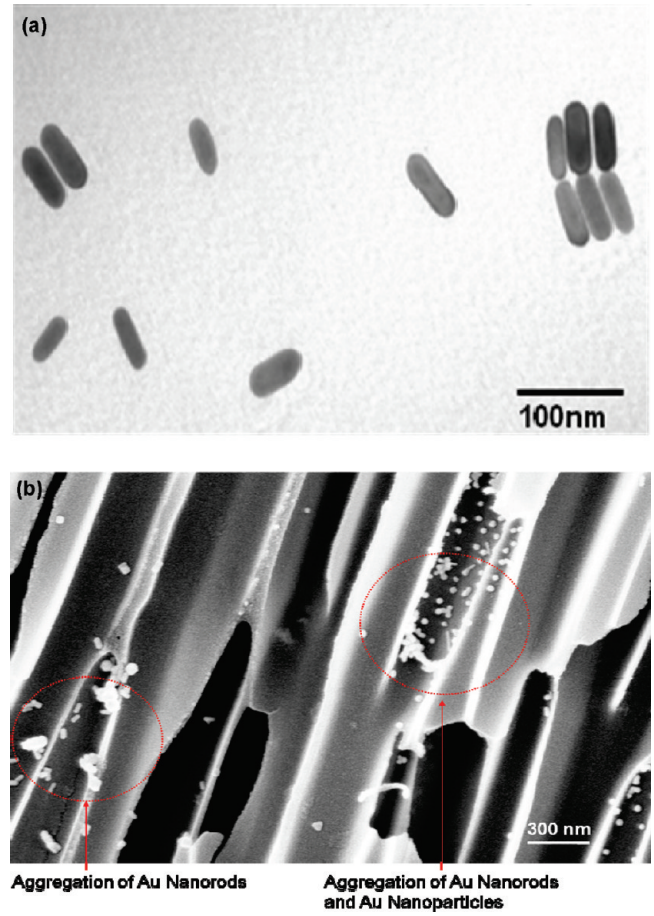

Figure 2. (a) TEM image of gold nanorods synthesized in this study. (b) SEM image of fractured porous alumina membrane with mixed gold nanorods and gold nanoparticles.

RESULTS AND DISCUSSION

Fabrication of SERS-Active Substrate. *Properties of Substrates.* The TEM image shows the presence of gold nanorods having an aspect ratio of ~4 with the a length of 80 ± 8 nm and a width of 19 ± 4 nm (Figure 2a). We utilized PAMs with a pore diameter of about 250 nm and a thickness of 60 μm for uniform distribution of gold nanorods and particles. If we use PAMs with a smaller pore size, the active surface area might increase and enhance SERS performance. However, because of the size of gold nanoparticles and nanorods, utilizing PAMs with a smaller pore diameter can cause pore blocking during loading and degrade SERS performance. The rationale behind choosing PAMs with a thickness of 60 μm is that the PAMs with thickness smaller than 60 μm are extremely brittle and difficult to handle and require multiple processing steps for chemical modification. On the other hand, because of finite transmission of light in PAMs (50% over 60 μm), thicker PAMs are not favorable.

The SEM image of the fractured PAMs loaded with mixed nanoparticles shows that both nanorods and nanoparticles were successfully immobilized on the polymer (PAN) coated side walls of PAMs (Figure 2b). We loaded about 32 μmol/cm^3 of mixed gold nanoparticles and gold nanorods into the PAM for the best SERS

(42) Kuptsov, H.; Zhizhin G. N. *Handbook of Fourier-transform Raman and infrared spectra of polymers A*; Elsevier: Amsterdam, 1998.
(43) Lin-Vien, D.; Colthup, N. B.; Fateley, W. G.; Grasselli, J. G. *The Handbook of Infrared and Raman Characteristic Frequencies of Organic Molecules*; Academic Press, Inc.: San Diego, 1991.

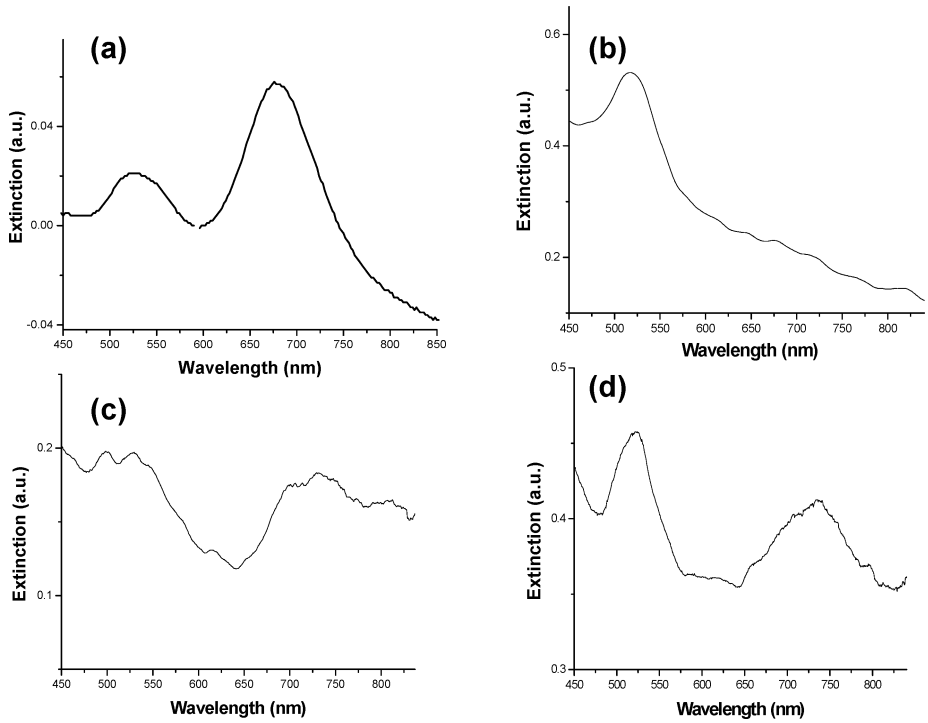

Figure 3. UV−vis extinction spectra of (a) gold nanorod solution, (b) PAM decorated with gold nanoparticles, (c) PAM with gold nanorods, and (d) PAM with mixed gold nanorods and gold nanoparticles.

performance as concluded in previous studies.[44,45] As we have already demonstrated, further increase in nanoparticle concentration reduces membrane transparency and SERS efficiency.[34,44]

It is well-known that the extinction spectrum of the gold nanorod solution exhibits two characteristic peaks related to transverse (520 nm) and longitudinal (680 nm) plasmon resonances (Figure 3a).[41] PAM substrate with gold nanoparticles shows its UV−vis extinction peak at 520 nm (Figure 3b), whereas substrate with gold nanorods exhibits a peak at 520 nm and a relatively broad peak around 700 nm (Figure 3c). The UV−vis extinction spectrum of SERS substrate with mixed gold nanorods and nanoparticles exhibits two characteristic peaks from gold nanorods and nanoparticles (Figure 3d). In the case of utilizing a 785 nm laser as an excitation source, gold nanorods and mixed gold nanorod−nanoparticles are expected to provide higher SERS enhancement because the longitudinal plasmon resonance of the nanorods and the coupled plasmon resonance of the aggregated nanoparticles overlaps with the wavelength of the excitation light.

Comparison of Various SERS Substrates. Considering very different optical absorption properties of gold nanostructures, we prepared three types of PAMs loaded with various nanostructures: gold nanorods, nanoparticles, and their 50:50 mixtures (Figure 4a−c). Apparently, gold nanorods were distributed and aggregated in end-to-end orientation through the cylindrical pores of PAMs. In contrast, gold nanoparticles and mixed nanostructures formed clusters with very few (5−10) units in a single cluster.

Raman spectra were obtained from PAMs loaded with various types of nanostructures after deposition of 100 ppm of HMTD solution. The Raman spectra for bare PAMs and PAMs loaded with gold nanoparticles or gold nanorods showed very low

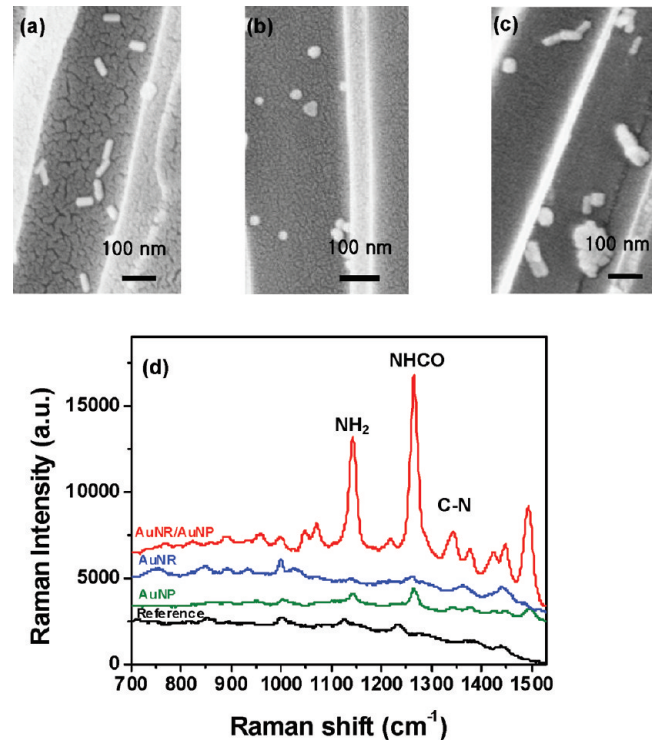

Figure 4. SEM images of (a) PAM substrate with gold nanorods, (b) PAM substrate with gold nanoparticles, and (c) PAM substrate with mixed gold nanorods and gold nanoparticles. (d) Comparison of Raman spectra of HMTD obtained with PAM substrates with mixed gold nanorods and gold nanoparticles, gold nanorods, gold nanoparticles, and PAM without HMTD. (Black line corresponds to reference spectrum.)

intensities (Figure 4d). In contrast, the overall intensity of Raman spectra (peak assignment will be discussed later) from PAM

(44) Ko, H.; Chang, S.; Tsukruk, V. V. *ACS Nano* **2009**, *3*, 181–188.
(45) Xu, J.; Xia, J.; Wang, J.; Shinar, J.; Lin, Z. *Appl. Phys. Lett.* **2006**, *89*, 133110–3.

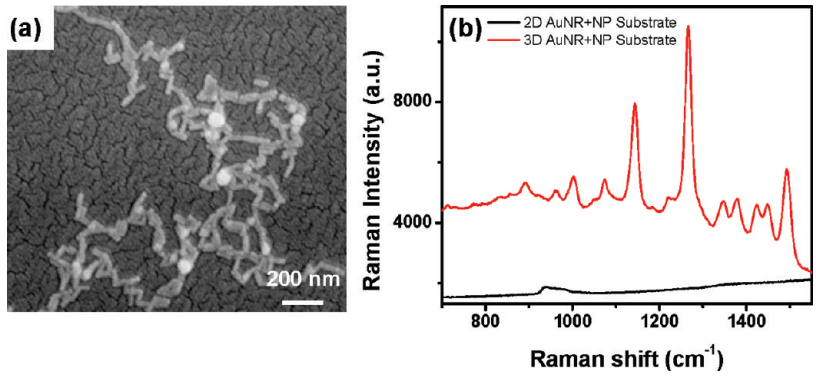

Figure 5. (a) SEM image of 2D SERS substrate comprised of gold nanoparticles and gold nanorods. (b) Raman spectra of 100 ppm of HMTD on planar and nanoporous 3D substrates.

substrates loaded with mixed gold nanorods and gold nanoparticles was one order of magnitude higher compared to the PAM loaded with gold nanoparticles alone or gold nanorods alone (Figure 4d). The enhanced performance of the SERS substrate with mixed gold nanorods and gold nanoparticles might be related to two different effects. First, the wavelength of the near IR laser (785 nm) nearly overlaps the longitudinal plasmon absorption (680 nm) of gold nanorods, resulting in strong electromagnetic field.[33] Second, it is known that the multishape, multisize particle aggregates exhibit higher enhancement compared to uniform particle aggregates.[46] Aggregation of the nanoparticles and the nanorods results in "hot" interstices which host extremely large electromagnetic fields and hence large SERS enhancement.

For instance, recently, our group has demonstrated that the SERS enhancement from a nanowire/nanoparticle hybrid structure (silver nanowires decorated with gold nanoparticles) is nearly 2 orders higher compared to that for the individual nanoparticles or the nanowires.[47] Even though SERS substrate with gold nanorod alone has UV−vis extinction overlapping near 785 nm wavelength (Figure 3c), the performance of the SERS substrate with gold nanoparticles is better than that for PAMs with gold nanorods alone, which can be explained by the enhancement effect due to the alignment of the aggregated gold nanorods and coupling within gold nanoparticle clusters (Figure 4).

In fact, gold nanorods are distributed and aggregated in end-to-end orientation through the cylindrical pores of the membrane, which is caused by the unidirectional flow of solution in the course of vacuum filtration (Figure 4a). The oriented aggregates of gold nanorods exhibit a red-shift and significant broadening of the longitudinal plasmon peak resulting in weak enhancement (Figure 3c).[48,49] On the other hand, in the case of gold nanoparticle aggregates the coupled plasmon resonance (nearly 700 nm) is relatively weak but close to the excitation wavelength (785 nm), resulting in much higher SERS enhancement compared to the aggregated nanorods. Such aggregation of the gold nanoparticles is favorable for large SERS enhancement owing to the large capacitive fields in their interstices.[34] In the case of mixed gold nanostructures, gold nanorods do not orient along the canal because of the presence of gold nanoparticles (sequential infiltration), which exhibit red-shift (nearly 720 nm). As a result of this, the coupled plasmon resonances induce a large SERS enhancement well above that observed for individual nanoparticles and aggregates of gold nanoparticles utilized in our previous publications (Figure 3d).[34,44]

We also compared the 3D and 2D substrates with similar aggregates of gold nanorods and nanoparticles. The SEM image shows gold nanorods and gold nanoparticles assembled on a PAN-coated silicon substrate (Figure 5a). As has been observed, the planar substrate showed no significant Raman enhancement even with relatively high concentration of HMTD (100 ppm). This direct comparison underscores the favorable attributes (enhanced surface area, efficient light interaction, and high density of hot spots) of the 3D nanocanal array with mixed gold nanorods and nanoparticles (Figure 5b).

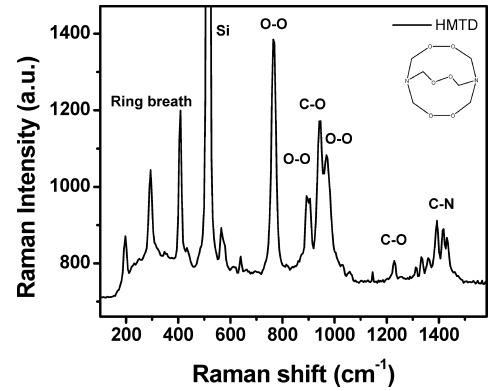

Figure 6. Raman spectrum of bulk HMTD on a silicon substrate with peak assignments; inset shows chemical structure of HMTD molecule.

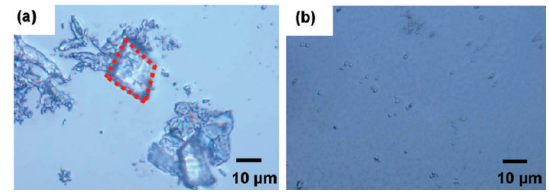

Figure 7. Bright field optical images of HMTD (a) on a silicon substrate and (b) on polyacrylonitrile coating.

(46) Camden, J. P.; Dieringer, J. A.; Wang, Y.; Masiello, D. J.; Marks, L. D.; Schatz, G. C.; Van Duyne, R. P. *J. Am. Chem. Soc.* **2008**, *130*, 12616–7.
(47) Gunawidjaja, R.; Peleshanko, S.; Ko, H.; Tsukruk, V. V. *Adv. Mater.* **2008**, *20*, 1544–1549.
(48) Willets, K. A.; Van Duyne, R. P. *Annu. Rev. Phys. Chem.* **2007**, *58*, 267–297.
(49) Sun, Z.; Ni, W.; Yang, Z.; Kou, X.; Li, L.; Wang, J. *Small* **2008**, *4*, 1287–1292.

Scheme 1. Proposed Path for Photocatalytic Decomposition of HMTD Molecule on Selected Nanocoatings

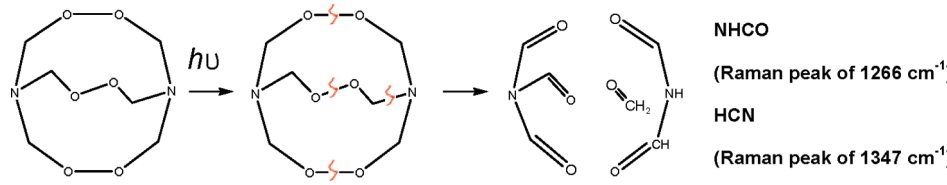

Table 1. Parameters of Various Bonds in HTMD Molecule[59]

	bond length (pm)	bond energy (kJ/mol)
O−O	148	145
C−C	154	348
C−O	143	360
C−N	147	308
C≡N	116	891

Analysis of the SERS Spectra. Preliminary Raman measurements were performed at low laser power in order to avoid photodecomposition which might cause the dissociation of HMTD molecules.[50,51] However, no observable Raman bands were obtained at low laser power (<10 mw), and thus a conventional, nondestructive SERS approach cannot be utilized for the chemical sensing of this peroxide even at relatively high concentration. To resolve this issue, we adapted an alternate approach, which relies on the photocatalytic decomposition of HMTD with higher power laser irradiation followed by the analysis of the Raman bands of the products for the fingerprint.

To study the molecular structure and characteristic features of Raman spectra of intact HMTD, we conducted Raman measurement of bulk HMTD and assigned Raman peaks to particular group vibrations. Raman spectra of the bulk material reveals strong characteristic peaks of HMTD at 769 cm^{-1} of O−O stretching band and at 950 cm^{-1} of C−O stretching band (Figure 6).[52] The positions of these peaks and other bands agree well with previous experimental Raman spectra of bulk HMTD material and can be assigned to different HMTD fragments as presented in Supporting Information (Figure S1).[52]

Raman spectra collected in a nondestructive mode with the laser intensity of 10 mW showed peaks at 1143 cm^{-1}, 1266 cm^{-1}, and 1347 cm^{-1} (Figure 4d). Strong Raman peaks at 1143 cm^{-1}, 1266 cm^{-1}, and 1347 cm^{-1} do not appear in the Raman spectrum of bulk HMTD. We speculate that these drastically enhanced Raman signatures of HMTD on our SERS substrate originated from corresponding decomposed fragments of HMTD molecules as will be discussed later.

Selective Coating To Control HMTD Adsorption and Decomposition. Proper selection of the modification routines and materials for PAM chemical modification are critically important for controlling HMTD adsorption from solution. Efficient dispersion of the molecules over a large area requires the modification of the alumina surface with a selective coating. As known, HMTD is a crystalline solid and it tends to crystallize during the process of solvent evaporation when cast from solution directly on the oxide surface thus preventing fine distribution along cylindrical pores (Figure 7a).[53]

For a proper selective polymer coating for HMTD adsorption, we explored various polyelectrolytes such as poly(acrylic acid) (PAA), poly(diallyldimethyl ammonium chloride) (PDDA), and polyethylenimine (PEI). None of these polymer coatings gave any characteristic Raman peak enhancement even with 100 ppm level of HMTD (Figures S2). Finally, polyacrylonitrile (PAN) coating was observed to be a good selective coating which suppresses crystallization and provides the means for uniform HMTD adsorption. This is confirmed by a simple drop and evaporation test of HMTD on a 5 nm PAN layer, demonstrating uniform coverage without any crystallization and aggregation (Figure 7b). Thus, a PAN coating was employed as a selective coating for the inner walls of pores in further studies. It is worth noting that gold nanorods and nanoparticles attached to the PAMs have been coated with an additional PAN layer with a thickness of about 2 nm. The thickness of the PAN layer employed here as a protective coating was sufficiently small to preserve the electromagnetic enhancement of the gold nanostructures.[54]

We suggest that PAN coating is the most appropriate because polar bonds of HMTD molecules tend to withdraw electrons from the nitrogen atoms, making C−N−C bonds more electron deficient and enabling efficient interaction with electron-donating cyanide groups of PAN.[34,55] Moreover, HMTD exhibits high solubility in acetonitrile (δ = 24.6 $MPa^{1/2}$); thus, solubility parameters of HMTD and PAN (δ = 25.3 $MPa^{1/2}$) should be very similar. The close values of solubility parameter indicates a high partition coefficient between HMTD and PAN, providing for easy solubility.

Raman Analysis of HMTD on SERS Substrates. *Raman Peak Assignment.* The presence of Raman peaks which cannot be assigned to intact HMTD molecules suggests the possibility of either strong interaction between HMTD and a selective coating or laser-induced photocatalytic decomposition of HMTD or both. Because strongly enhanced peaks (1143 cm^{-1}, 1266 cm^{-1}, and 1347 cm^{-1}) do not appear in the Raman spectrum of bulk HMTD, we speculate that these drastically enhanced peaks originate from decomposed compounds of HMTD molecules. Thermal decomposition can be considered as the way to verify decomposed materials of HMTD. Indeed, T-jump/FT-IR spectroscopy has been employed to analyze the thermally decomposed compounds of HMTD.[56] It was found that the decomposed materials are primarily comprised of CO gas (78 mol %), and small amounts of HCN, HNCO, and CH_4. While

(50) Joy, V. T.; Srinivasan, T. K. K. *J. Mol. Struct.* **2000**, *516*, 225–230.
(51) Sun, S.; Birke, R. L.; Lombardi, J. R.; Leung, K. P.; Genack, A. Z. *J. Phys. Chem.* **1988**, *92*, 5965–5972.
(52) Oxley, J.; Smith, J.; Brady, J.; Dubnikova, F.; Kosloff, R.; Zeiri, L.; Zeiri, Y. *Appl. Spectrosc.* **2008**, *62*, 906–915.
(53) Schaefer, W. P.; Fourkas, J. T.; Tiemann, B. G. *J. Am. Chem. Soc.* **1985**, *107*, 2461–2463.
(54) Pettinger, B.; Domke, K. F.; Zhang, D.; Schuster, R.; Ertl, G. *Phys. Rev. B* **2007**, *76*, 113409–113413.
(55) Thery-Merland, F.; Methivier, C.; Pasquinet, E.; Hairault, L.; Pradier, C. M. *Sens. Actuators, B* **2006**, *114*, 223–228.
(56) Hiyoshi, R. I.; Nakamura, J.; Brill, T. B. *Prop. Explos. Pyrotech.* **2007**, *32*, 127.

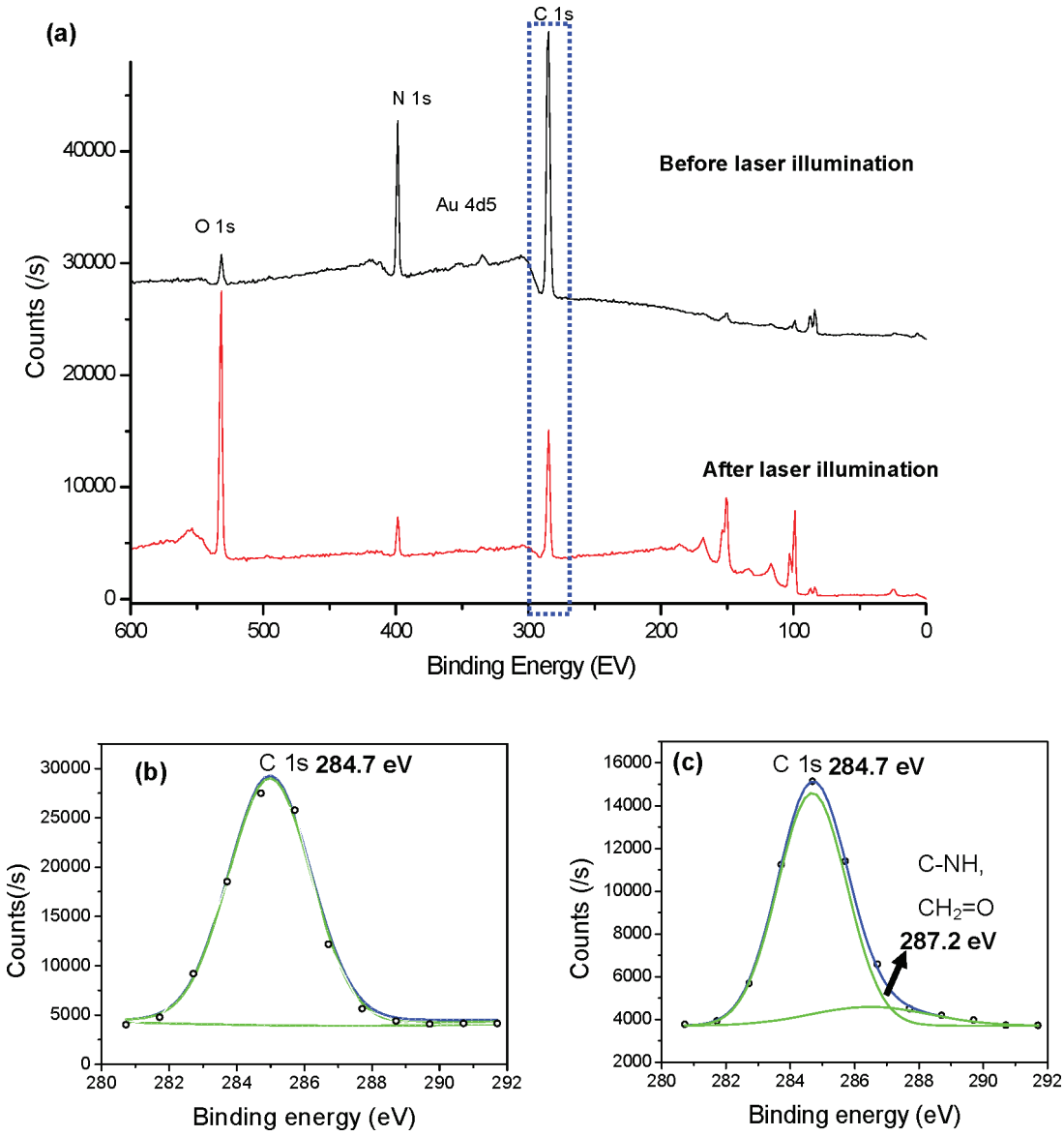

Figure 8. (a) XPS spectra of HMTD before and after laser irradiation, and XPS spectra of C 1s peak deconvolution of HMTD and assigned bonds (b) before laser irradiation and (c) after laser irradiation.

CO is a gaseous product, other solid debris are considered as the major contribution of Raman peaks. As can be seen in Figure 4d, a relatively strong peak at 1266 cm^{-1} might arise from the molecules containing HNCO group, and the peak at 1143 cm^{-1} arises from the NH_2 rocking vibration.[42,43] Multiple amine vibrations are present between 1310 cm^{-1} and 1360 cm^{-1}.[42,57,58] (Figure S1, Table S1).

We propose that the strong Raman bands observed here originate from the photodecomposition of HMTD molecules caused by laser-induced bond cleavage as shown in Scheme 1. Decomposed fragments can be suggested by considering the possible bond cleavage depending on the specific bond energy level.[56,59] The various bond energies for HMTD molecules (Table 1) shows that the lowest bond energy corresponds to the O−O (peroxide) bond (145 kJ/mol).[56] Thus, we suggest that photocatalytic reaction initiated by laser illumination should first result in the cleavage of the peroxide bonds in HMTD, generating radicals (Scheme 1).[37,60−62] Another possible cleavage could occur on C−N bond (308 kJ/mol), resulting in fragmented compounds containing a HNCO group, which possess a strong Raman band at 1266 cm^{-1}.[42,43]

To clarify the decomposed material of HMTD, we perform X-ray photoelectron spectroscopy (XPS) of HMTD on gold nanoclusters with a selective coating before and after laser irradiation (785 nm). The plot in Figure 8b shows the XPS spectrum from PAN+AuNP+PAN+HMTD sample and the same

(57) Peña-Quevedo, A. J.; Mina-Calmide, N.; Rodríguez, N.; Nieves, D.; Cody, R. B.; Hernández-Rivera, S. P. *Proc. SPIE* **2006**, *6201*, 62012E/1−10.
(58) Peña-Quevedo, A. J.; Figueroa, J.; Rodríguez, N.; Nieves, D.; Hernández, N.; Rivera, R.; Mina, N.; Hernández-Rivera, S. P. *Proc. SPIE* **2006**, *6201*, 62012D/1−8.
(59) Cottrell, T. L. *The Strengths of Chemical Bonds*, 2nd ed.; Butterworths: London, 1958.

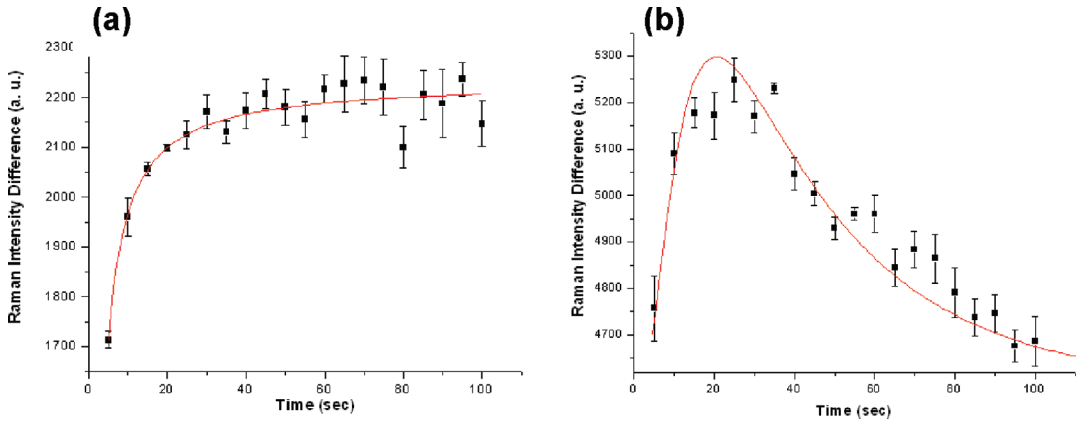

Figure 9. (a) The intensity of Raman peak at 1266 cm^{-1} as a function of illumination time with laser power of 10 mW (a) and 20 mW (b).

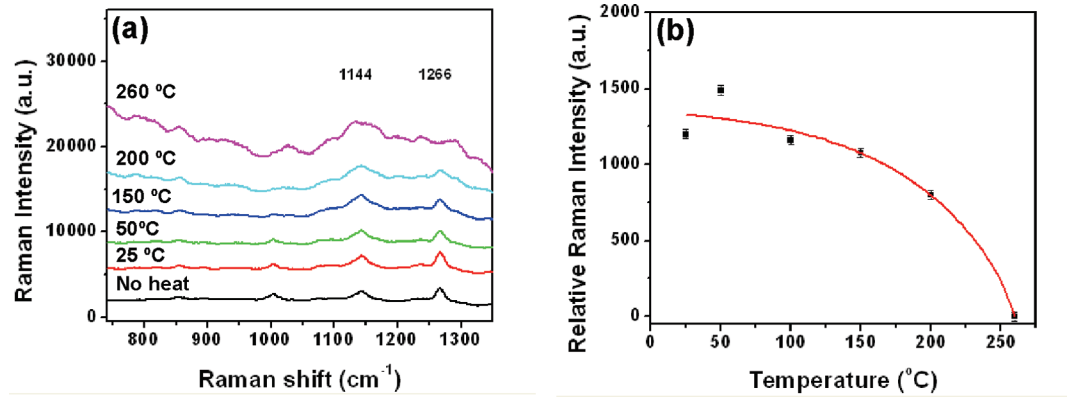

Figure 10. (a) Raman spectra collected after temperature treatment. (b) Relative Raman intensity at 1266 cm^{-1} as a function of temperature treatment.

after laser irradiation. The XPS spectrum clearly showing the C 1s, O 1s, N 1s, Au 4d5 corresponding to chemical composition of the samples (Figure 8a).[63] After laser illumination we observed a significant increase in the oxygen band which indicates intense oxidation processes. Of particular interest is the C 1s band (284.7 eV) of the HMTD after the laser irradiation. After laser illumination, this band shows a weak shoulder at 287.2 eV as opposed to the band before laser irradiation which shows no signs of such shoulder (Figure 8b,c). The presence of additional contribution at 287.2 eV indicates the presence of C−NH, CH_2=O, and NH_2−C=O fragments (positions within 287−289 eV) that can only be generated by the O−O and C−N bond cleavage of HMTD molecules, which is the proposed path for the photocatalytic decomposition of the HMTD molecule (Scheme 1).[63,64]

We suggest that the presence of gold nanoparticles and nanorods might augment the photoinitiated decomposition of the HMTD. Indeed, as known, gold nanoparticles exhibit significant photocatalytic activity under laser irradiation.[65] Specifically, the presence of gold nanoparticles causes the increase of quantum yield of photocatalytic decomposition process.[66] To confirm the photocatalytic decomposition of HMTD we monitored the variation of Raman intensity at 1266 cm^{-1} as a function of illumination time at different laser powers (Figure 9a). Raman spectra collected every 5 s at 10 mW of laser power showed that the intensity of the Raman peak monotonically increases over the first 40 s followed by saturation. In contrast, when a higher laser power (20 mW) was used, Raman intensity at 1266 cm^{-1} exhibited faster initial increase followed by a decay, indicating complete photodecomposition of HMTD fragments (Figure 9b). These Raman measurements indicate that HMTD molecules on the gold nanoparticle surfaces can be indeed photocatalytically decomposed by the laser irradiation as has been suggested in related studies.[25] Moreover, FTIR measurement also showed decomposition of initial HMTD material after thermal treatment (Supporting Information).

Moreover, during Raman measurement, an excitation laser can increase local temperature of the specimen and lead to Raman band changes.[67,68] During laser illumination on gold nanoparticle

(60) Beltran-Heredia, J.; Torregrosa, J.; Dominguez, J. R.; Peres, J. A. *Ind. Eng. Chem. Res.* **2001**, *40*, 3104–3108.
(61) Ling, P.; Boldyrev, A. I.; Simons, J.; Wight, C. A. *J. Am. Chem. Soc.* **1998**, *120*, 12327–12333.
(62) Song, W.; Ravindran, V.; Pirbazari, M. *Chem. Eng. Sci.* **2008**, *63*, 3249–3270.
(63) Okpalugo, T. I. T.; Papakonstantinou, P.; Murphy, H.; McLaughlin, J.; Brown, N. M. D. *Carbon* **2005**, *43*, 153–161.
(64) Moulder, J. F.; Stickle, W. F.; Sobol, P. E.; Bomben. K. D. *Handbook of X-ray Photoelectron Spectroscopy*; Chastain, J., Ed.; Perkin-Elmer Corporation: Eden Prairie, 1992.
(65) Kama, P. V. *J. Phys. Chem. B* **2002**, *106*, 7729–7744.
(66) Iliev, V.; Tomova, D.; Bilyarska, L.; Tyuliev, G. *J. Mol. Catal. A: Chem.* **2007**, *263*, 32–38.
(67) McNesby, K. L.; Fell, N. F., Jr.; Vanderhoff, J. A. *Proc. SPIE* **1997**, *3082*, 121–135.

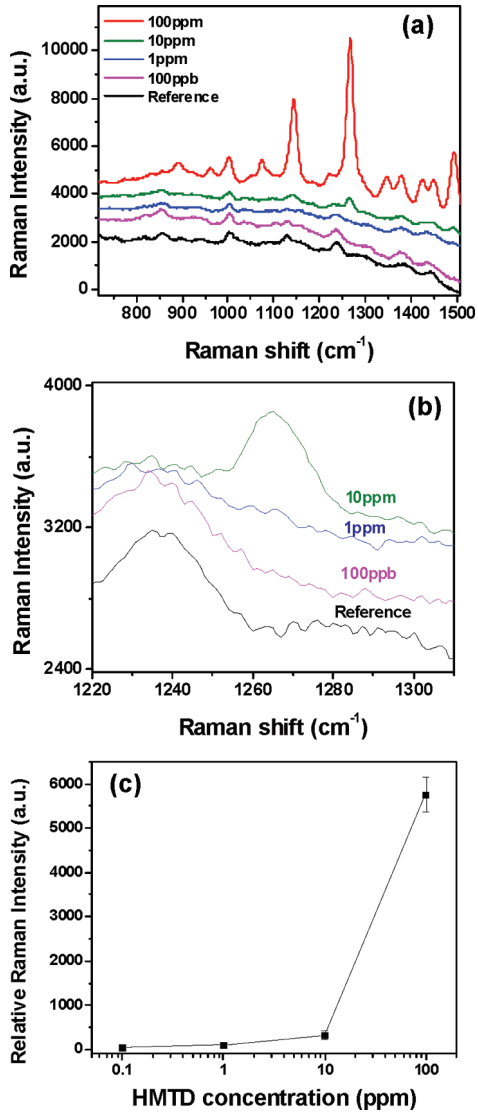

Figure 11. (a) Raman spectra of different concentrations of HMTD on SERS substrate coated; reference spectrum is for PAM without HMTD. (b) Raman spectra at 1266 cm^{-1} with different concentrations of HMTD. (c) Raman intensity at 1266 cm^{-1} vs HMTD concentration.

aggregates, nanoparticles absorb light energy and convert it to heat (because of nonradiative relaxation by electron−lattice phonon interaction) which also can contribute the decomposition of HMTD.[69] To test the role of thermal decomposition, we conducted in situ Raman measurement during heating of the SERS substrate with HTMD molecules (Figure 10a).[56,70] From the plot it is clear that the NHCO fragments are stable at modest temperature, but above 200 °C these fragments evaporate and the Raman band consequently disappears (Figure 10b).

Monitoring of Trace Amounts of HMTD. To estimate SERS enhancement and the ultimate chemical sensing with the SERS substrate, Raman spectra were collected and averaged over four different locations on a 1 cm^2 area of the SERS substrate (Figure 11a). Raman spectra showed all major features discussed above with the intensity of the main peak at 1266 cm^{-1} increasing with the increase of HMTD concentration. High resolution spectra in the range 1220−1300 cm^{-1} show a strong peak at 1266 cm^{-1} for HMTD concentrations down to 10 ppm and a relatively weak peak (SNR of ~2) for a concentration of 1 ppm. Interpolating from the SNR at 10 ppm and 1 ppm, we estimate the limit of detection (LOD) to be ~3 ppm for a detectable signal-to-noise ratio of higher than 3 (Figure 11b). This concentration corresponds to about 2 pg of HMTD within the laser footprint (30 μm of diameter). This detectable amount is about 3 orders of magnitude lower than currently reported LOD, which is 1 ng as determined with mass spectroscopy.[18]

CONCLUSION

In conclusion, we suggest a novel method for the fast detection of HMTD molecules utilizing photocatalytic decomposition of the molecules and analyzing the resulting chemical fragments using SERS. The SERS-active substrate has been successfully fabricated by decorating inner walls of porous membranes with mixed gold nanorod−nanoparticle clusters, which provide "hot spots" with plasmon resonance close to the laser excitation. We demonstrated that the 3D PAM substrates can give a strongly enhanced Raman signal from the photodecomposed fragments of HMTD, providing truly trace detection with sensitivity exceeding that of earlier reports by several orders of magnitude.

We believe that the design of robust, inexpensive, and readily available nanoporous SERS substrates can be utilized for other peroxide-based explosives or different chemical analytes with proper modification of the selective nanocoating and nanostructures on inner walls. Moreover, the novel design of a nanoporous SERS substrate combined with the photodissociation detection approach introduced here is highly promising for monitoring "invisible", unstable, or metastable chemical compounds.

ACKNOWLEDGMENT

We thank Prof. Mohan Srinivasarao and Minsang Park for providing access to the Raman instrument, Dr. Eugenia Kharlampieva for TEM imaging, and Prof. Valery Shevchenko, Dr. Veronika Kozlovskaya, Dr. Hangi Chae, and Maneesh Gupta for technical support. This work was supported by NSF, DHS, ARO, and DARPA.

SUPPORTING INFORMATION AVAILABLE

Peak assignment of HMTD using ACD program; polymer selective coating on 3D SERS substrate for HMTD; FTIR analysis of HMTD. This material is available free of charge via the Internet at http://pubs.acs.org.

Received for review March 13, 2009. Accepted May 27, 2009.

AC900537D

(68) Pallone, A.; Sacchetti, A.; Corridoni, T.; Postorino, P.; Catelli, R.; Rousse, G.; Masquelier, C. *Solid State Ionics* **2004**, *170*, 135–138.
(69) Skirtach, A. G.; Karageorgiev, P.; Beidard, M. F.; Sukhorukov, G. B.; Mohwald, H. *J. Am. Chem. Soc.* **2008**, *130*, 11572–11573.
(70) Perez-Ramirez, J.; Mul, G.; Moulijn, J. A. *Vib. Spectrosc.* **2001**, *27*, 75–88.